

Intermittency in the photosphere and corona above an active region

Valentyna Abramenko

Big Bear Solar Observatory, 40386 N. Shore Lane, Big Bear City, CA 92314

Vasyl Yurchyshyn

Big Bear Solar Observatory, 40386 N. Shore Lane, Big Bear City, CA 92314

Haimin Wang

Center for Solar-Terrestrial Research, New Jersey Institute of Technology, 323 Martin

Luther King Boulevard, 101 Tiernan Hall, Newark, NJ 07102

Big Bear Solar Observatory, 40386 N. Shore Lane, Big Bear City, CA 92314

ABSTRACT

Recent studies undoubtedly demonstrate that the magnetic field in the photosphere and corona is an intermittent structure, which offers new views on the underlying physics. In particular, such problems as the existence in the corona of localized areas with extremely strong resistivity (required to explain magnetic reconnection of all scales) and the interchange between small and large scales (required in study of the photosphere/corona coupling), to name a few, can be easily captured by the concept of intermittency. This study is focused on simultaneous time variations of intermittency properties derived in the photosphere, chromosphere and corona. We analyzed data for NOAA AR 10930 acquired between Dec 08, 2006 12:00 UT and Dec 13, 2006 18:45 UT. Photospheric intermittency was inferred from Hinode magnetic field measurements, while intermittency in the transition region and corona was derived from Nobeyama 9 GHz radio polarization measurements, high cadence Hinode/XRT/Be-thin data as well as GOES 1-8Å flux. Photospheric dynamics and its possible relationship with the intermittency variations were also analyzed by calculating the kinetic vorticity. For this case study we found the following chain of events. Intermittency of the photospheric magnetic field peaked after the specific kinetic vorticity of plasma flows in the AR reached its maximum level (4 hour time delay). In turn, gradual increase of coronal intermittency occurred after the peak of the photospheric intermittency. The time delay between the peak of photospheric intermittency and the occurrence of the first strong (X3.4) flare was approximately 1.3 days. Our analysis seems to suggest that the enhancement of intermittency/complexity first occurs in the photosphere and is later transported toward the corona.

Subject headings: Sun: magnetic field; photosphere; corona

1. Introduction

It is a widely spread view that eruptive processes of energy release in the corona are seemingly independent of the dynamics observed in the moderately-varying photosphere. This view is partially based on the fact that no one-to-one correlation was observed between coronal and photospheric dynamics. For example, numerous attempts to find any persistent *pre*-flare changes in the photosphere did not lead to any solid conclusions yet. Although, recent efforts to detect flare-related changes in the photospheric magnetic fields were more successful (Spirock et al. 2002; Wang et al. 2004; Sudol & Harvey 2005; Wang 2006). More than a dozen publications by different research groups reported that persistent abrupt changes in the photospheric magnetic flux occur in association with X-class flares. The most plausible explanation of the observed phenomenon seems to be flare-related changes of the inclination of field lines rooted in the photosphere. If this is the case (future analysis of high cadence vector magnetograms could be helpful), then we probably deal with a feedback to the photosphere of reorganizing coronal fields.

The question whether there is any forward reaction of the photosphere toward the corona is still open, however. There seems to be some acceptance that a *statistical* relationship may exist between the conditions in the photosphere and corona: for a large enough statistical ensemble of active regions a good correlation has been found between photospheric magnetic parameters and coronal phenomena (Fisher et al. 1998; Falconer et al. 2003; Schrijver et al. 2004; Abramenko 2005a; McAteer et al. 2005; Schrijver & Title 2005; Abramenko et al. 2006; Jing et al. 2006; Tan et al. 2007; Leka & Barnes 2007 and references in; Georgoulis et al. 2007; Conlon et al. 2007). From a theoretical standpoint the consensus seems to be reached that the ultimate source of energy for coronal energy release is the photospheric and sub-photospheric motions of magnetized plasma. Various mechanisms have been suggested for the energy transport toward the corona that can and should be observationally validated (see reviews of coronal heating mechanisms, e.g., Malara & Velli 1994; Schrijver & Title 2005; Klimchuk 2006). Although, various statistical correlations do not seem to be adequate any longer and timing characteristics are required.

Indeed, when we address issues of coupling between any two systems, a question of vital importance immediately arises: do events that occur in one system persistently precede or follow events in another system? If the answer is “yes” then what is the characteristic time

delay between a pair of related events? A shorter delay suggests a more close and intimate coupling, while long time delays may indicate less straightforward and more complex relationship. In particular, in such dynamical systems as magnetized turbulent plasma, the interplay between scales may influence the delay time. In this case it is advantageous to adopt an intermittency approach, a technique that allows capturing interactions between various scales, in the best way possibly as of today. In the present study, we undertook an attempt to detect the delay intervals between key moments of the intermittency behavior in the photosphere and corona.

2. Data Analysis

High spatial and temporal resolution measurements of the photospheric magnetic field and solar corona performed recently by a set of *Hinode* instruments (Kosugi et al. 2007) provide us with a unique opportunity to simultaneously estimate degree of intermittency in the photosphere and corona and to track their variations in time.

Hinode SOT/FG instrument is designed to produce filter-based vector magnetograms at high spatial and temporal resolution. Strictly speaking, these images only represent measurements of the Stokes V polarization parameters at a single wavelength so that information on the magnetic field intensity is not available in these data. However, these data do bear information on the magnetic structuring with an unprecedented spatial resolution of 0.16 arcsec. These uninterrupted measurements are taken with a high time cadence of 2 minutes and cover several days of observations of an active region. An example of a SOT/FG/*Hinode* magnetogram for NOAA AR 10930 is shown in Figure 1 (*left*), while the right frame shows a simultaneous MDI/HR magnetogram recorded on the same area on the Sun. As far as spatial resolution is concerned, the advantage of the SOT/FG data is obvious.

We will analyze properties of photospheric intermittency by utilizing i) a flatness-function technique, which relates the slope of the function to the degree of intermittency and ii) calculations of the kinetic vorticity in the photosphere.

Three independent data sets were used to calculate the intermittency in the corona and chromosphere: X-ray emission records from the *Hinode*/XRT and GOES instruments as well as Nobeyama 9.4 GHz polarization flux.

We analyzed active region NOAA 10930 observed by *Hinode* in December 2006. During the passage across the solar disk, this active region displayed at least two periods of enhanced activity separated by a long interval of relative quietness. The first flaring

interval lasted from Dec 4 till Dec 7, 2006, when the active region was very close to the east limb. As evidenced from a series of MDI full disk magnetograms, at the end of this activity period the magnetic complexity in the active region was nearly exhausted and a new period of complexity gain was setting in. This second activity period was accompanied by gradual emerging of a fast-rotating sunspot of positive (N) polarity located in the close vicinity to the main negative polarity sunspot. The emergence and rotation of the sunspot ceased with the occurrence of two powerful X-class flares on Dec 13 and 14, 2006. The time period between Dec 8, 12:00 UT and Dec 13, 18:45 UT was chosen to study how time variations of magnetic complexity in the photosphere and corona are related.

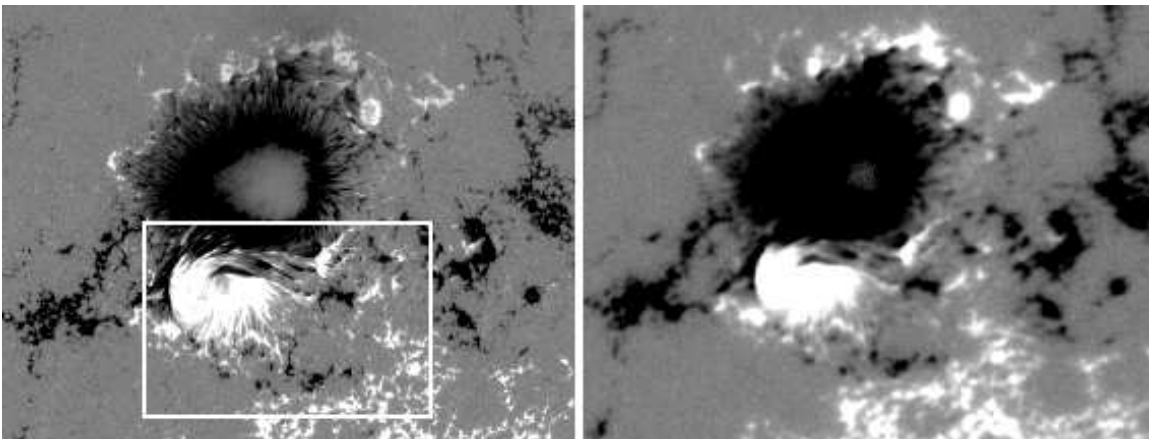


Fig. 1.— Line-of-sight magnetograms of NOAA 10930 recorded on 2006 Dec 12 at 00:48UT by SOT-FG/Hinode (*left*) and SOHO/MDI HR (*right*). MDI/HR (SOT/FG) magnetograms scaled between $-300...300$ G (DN). *The box* encloses an area used for calculations of the intermittency index, κ , and the squared kinetic vorticity, $\langle \omega^2 \rangle$.

We analyzed 1718 SOT/FG 2×2 re-binned magnetograms taken with the time cadence of 4 minutes. During the analyzed time interval the active region moved across the solar disk from longitude of E37 to W32, so that the influence of projection effect should be considered. We integrated longitudinal flux density, $|B_{\parallel}|$, over the entire number, N , of pixels of size $\Delta S = 0.32'' \times 0.32''$ occupied by the active region. We thus obtained the longitudinal total unsigned flux, Φ_{\parallel} , which is plotted in Figure 2 with the light blue curve. The assumption that the magnetic field in the photosphere is predominantly vertical to the solar surface offers a possibility to estimate the magnetic flux perpendicular to the solar surface, Φ_{\perp} (Murray 1992; Hagenaar 2001). For each magnetogram, we calculated the cosine of the angular distance from the center of the magnetogram to the solar disk center, $\cos\beta$ (Figure 2, pink curve). The perpendicular flux density thus can be estimated as $B_{\parallel}/\cos(\beta)$ and the deprojected pixel area is $\Delta S/\cos(\beta)$, which results in the estimated magnitude of the perpendicular unsigned flux $\Phi_{\perp} = \Phi_{\parallel}/\cos^2(\beta)$ (Figure 2, dark blue curve). Inside the

time range where $\cos(\beta) > 0.95$ (i.e., between the dashed vertical line segments in Figure 2) the perpendicular and longitudinal fluxes differ by less than 10%. We, therefore, accept that within this time range our data and results are essentially free from the projection effect.

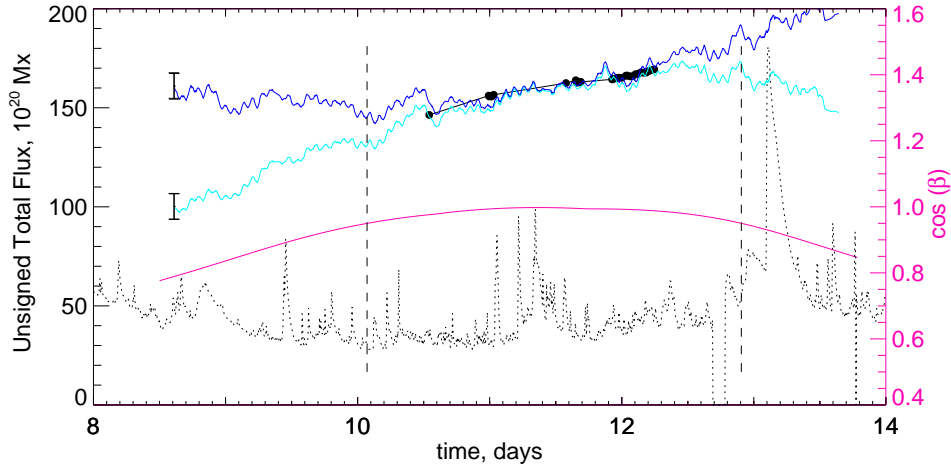


Fig. 2.— Time variation of the unsigned magnetic flux in NOAA 10930 calculated from SOT/FG magnetograms (arbitrary units): *light blue* - unsigned longitudinal flux, Φ_{\parallel} ; *dark blue* - unsigned perpendicular to the solar surface flux, Φ_{\perp} . The data points were smoothed by 35 point box car averaging. Typical error bars are shown. *Pink* - time variations of the cosine of the angular distance of the center of a magnetogram from the center of the solar disk, $\cos(\beta)$ (*left axis*). Inside the interval between two vertical dashed segments, where $\cos\beta > 0.95$, the projection effect is a minimum. *Dotted line* represents the GOES 1-8Å flux data. *Black circles* - longitudinal flux derived from MDI/HR magnetograms in units of 10^{20} Mx (*left axis*).

3. Measure of intermittency

Intermittency manifests itself in both spatial (2D or 3D) and temporal (1D) domains. In spatial domain, intermittency implies a tendency of the magnetic field to concentrate into small-scale flux tubes of high intensity, surrounded by extended areas of much weaker field. This tendency becomes more pronounced as the spatial resolution of data increases. In temporal domain, intermittency is evidenced via burst-like behavior of events. Studies of intermittency in both spatial and temporal domains can be conducted by using the same techniques such as the structure function approach (see, e.g., Frisch 1995).

Structure function, defined as statistical moments of the increment of a field, is a useful tool for exploring intermittency (Stolovitzky & Sreenivasan 1993; Frisch 1995; Consolini et al. 1999; Abramenko et al. 2002, 2003; Abramenko 2005b; Buchlin et al. 2006; Uritsky et al. 2007).

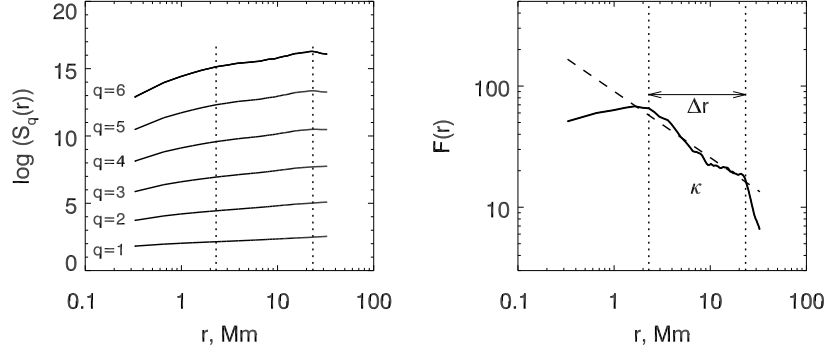


Fig. 3.— Structure functions $S_q(r)$ (Eq. (1), *left axis*) obtained from SOT/FG magnetogram shown in Figure 1 (*the box*). *Right* : - flatness function $F(r)$ derived from the structure functions (Eq.(2)). Vertical dotted lines mark the intermittency interval, Δr , where flatness grows according to the power law when r decreases. The interval Δr is also marked in the left frame. The intermittency index κ is the slope of $F(r)$ determined within Δr : the flatness function steepens as the magnetic field becomes more intermittent. For the shown magnetogram, $\kappa = 0.55 \pm 0.05$ was determined from the linear regression (*dashed line*) inside the range $\Delta r = (2.3 - 23)$ Mm.

In our case the analyzed field is the line-of-sight component, B_{\parallel} , of the photospheric magnetic field so that the structure function can be defined as:

$$S_q(r) = \langle |B_{\parallel}(\mathbf{x} + \mathbf{r}) - B_{\parallel}(\mathbf{x})|^q \rangle, \quad (1)$$

where \mathbf{x} is a current pixel on a magnetogram, \mathbf{r} is the separation vector and q is the order of a statistical moment, which takes on real values. Angular brackets denote averaging over the magnetogram.

As we mentioned earlier, ratio of the fourth statistical moment of the structure function to the square of the second statistical moment determines the flatness function. However, in the case of intermittency analysis Frisch (1995) suggested to use even higher statistical moments and to calculate the (hyper-)flatness, namely, ratio of the sixth moment to the cube of the second moment:

$$F(r) = S_6(r)/(S_2(r))^3 \sim r^{-\kappa}. \quad (2)$$

For non-intermittent structures, the flatness does not depend on the spatial scale, r . On the contrary, for an intermittent structure, the flatness grows as a power-law when the scale r decreases (Frisch 1995, Abramenko 2005b). The intermittency index, κ , determined as the slope of the flatness function within a spatial range of linearity, Δr (Figure 3), increases when intermittency is higher.

We applied the above technique to analyze intermittency in both spatial and temporal domains. To process 1D time series, we modified our 2D flatness function code based on Eqs.(1 - 2) by substituting spatial scale by time scale, τ , and magnetic field, B_{\parallel} , by time series of coronal measurements.

First, we determined the flatness functions and intermittency indices for all selected SOT/FG magnetograms. To avoid possible contamination of the results from the saturation effect inside the main sunspot and the vast area of weak fields around it, only the fields enclosed by the box in Figure 1 (fast rotating spot and flare site) were taken for calculations. The range $\Delta r = (2.3 - 23)$ Mm, as it is show in Figure 3, was taken the same for all magnetograms.

Double green curve in Figure 4 shows time profile of κ in the photosphere. The intermittency index peaked on Dec 11 at about 18:00UT (day 11.75), which is approximately 1.3 day before the X3.4 flare. This peak is located inside the projection-free time interval (between two vertical dashed line segments in Figure 4) and its magnitude significantly exceeds the error bar, which allows us to consider it as a real change in complexity of the photospheric magnetic field.

Second, to explore properties of intermittency in the solar chromosphere and corona, we utilized time series obtained from various instruments such as Hinode/XRT, GOES and Nobeyama radio-polarimeter. Both hard X-ray and radio fluxes are direct traces of electrons accelerated in reconnection events. Intermittency analysis based on these data may reveal information on the chromospheric and coronal reconnection dynamics, i.e., reorganization in the magnetic field.

We used 1 min Be-thin filter data taken with XRT/Hinode instrument (Kosugi et al. 2007, Golub et al. 2007). The XRT images were processed with the standard SSWIDL XRT software package and the XRT flux was calculated by integrating pixel intensities over the active region (Figure 5). The XRT data for this time interval are not continuous. We analyzed three sub-sets acquired on 9.4 - 10.4 day, 10.4-11.4 day, and 13.0 - 13.7 day. We denoted them as Dec 10, Dec 11, and Dec 13 data sets. Each subset contains about 1000 data points. For each sub-set, we calculated the flatness functions (Figure 6, *left*) and the intermittency index κ .

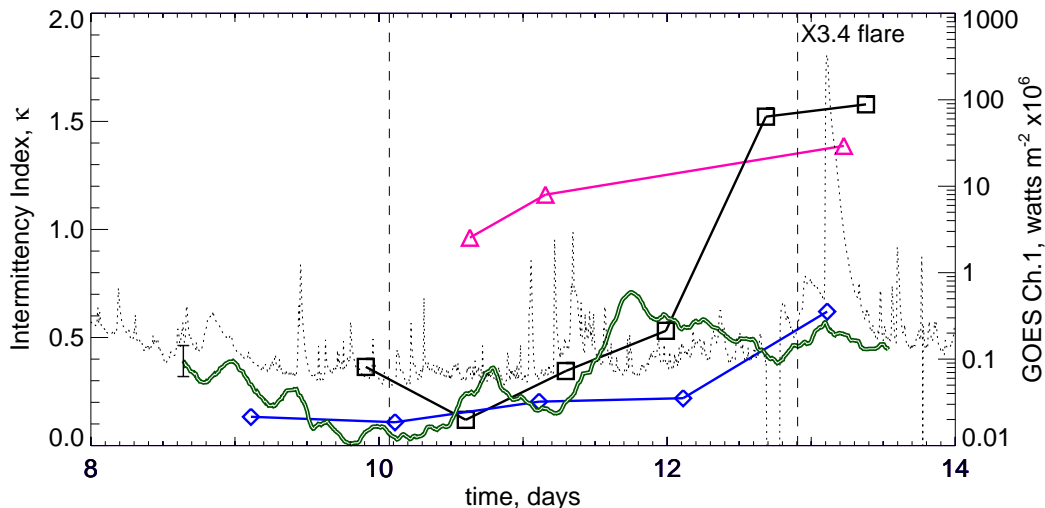


Fig. 4.— Time variations of the intermittency index, κ , determined from i) photospheric magnetograms (*double green line*, the data points were smoothed by 35 point box car averaging, and a typical error bar of smoothing is shown), ii) XRT data (*purple triangles*), iii) Nobeyama radio data (*blue diamonds*), and iv) GOES flux (*black squares*). For the last three cases, error bars are less than the symbol size. Other notations are the same as in Figure 2.

The data presented in Figure 6 allow to give an explanation how we select a linear interval, Δr , for the time series. In each case, a linear range was detected in the middle part of a spectrum. We then extended this range in both directions and recalculated the linear fit and the slope, κ . We continued to do so while deviations of κ remained inside the standard deviation of the linear fit, which was in the most of the cases less than 0.05.

Polarization flux at 9.4 GHz from Nobeyama radioheliograph is shown in Figure 5. The radio emission at this frequency is predominantly determined by the gyro-resonance process and is largely controlled by the strength and dynamics of the magnetic field above active regions (Kundu 1965; Aschwanden 2002). We re-binned these 1-second data, so that new time sampling was 30 seconds, and calculated the flatness function for each observing day thus obtaining 5 estimations of $F(\tau)$. Three of them are presented in Figure 6 (*right*). The corresponding values of κ are shown in Figure 4.

As evidenced from both XRT and Nobeyama data (Figure 6), the slope of the flatness function gradually steepened from Dec 10 to Dec 13, implying a gradual increase of intermittency. One more interesting detail can be noted in behavior of $F(\tau)$. Namely, the large-scale end of the linear interval (i.e., interval of scales involved into intermittent

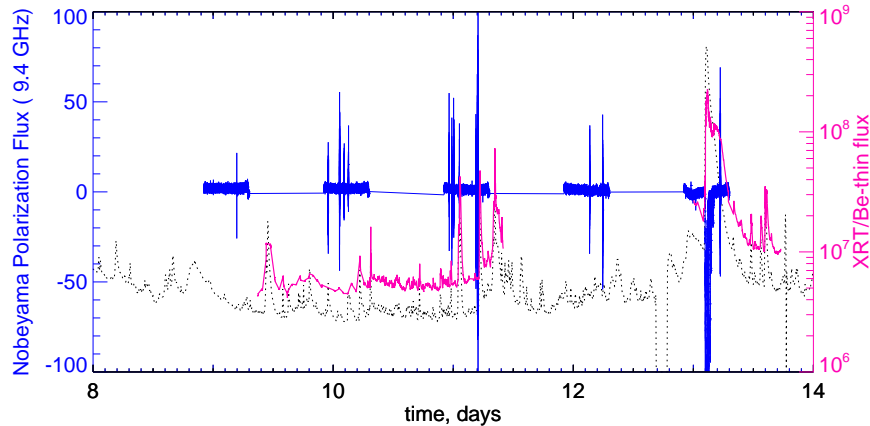


Fig. 5.— *Purple* - Time variations of the XRT/Hinode Be-thin flux integrated over the active region area. *Blue* - time variations of the radio polarization flux at 9.4 GHz from Nobeyama radioheliograph. *Dotted* line represents GOES flux.

process) shifts toward the larger scales as κ increases (see the functions for Dec 13). It means that growing intermittency (complexity) involves increasingly larger time scales. Note that similar behavior (involvement of larger spatial scales) we also observed in the case of the photospheric magnetic field.

The same intermittency calculation routines were applied to the six one-day time series of 1-minute GOES 1-8 Å flux.

In Figure 4 we compare the time variations of the intermittency indices in the photosphere, chromosphere and corona. Photospheric data show an undulating behavior with a prominent peak on Dec 11 and a gradual decrease after that, while coronal and chromospheric indices continue to increase through Dec 13. Thus the data seem to suggest that intermittency may first increase in the photosphere and then propagates toward the chromosphere and corona.

What processes in the photosphere and beneath are responsible for this gain of complexity and intermittency? It is thought that convective and turbulent motions of the magnetized plasma in photospheric and sub-photospheric layers could be responsible for the increasing complexity (see, e.g., review by Klimchuk 2006). Statistical comparisons (e.g., Abramenko et al., 2006; Jing et al., 2006; Tan et al., 2007) seem to agree with this assumption. If so, photospheric dynamics could be compared to the intermittency indices, and the attention should be focused on the kinetics of the photospheric magnetic flux tubes.

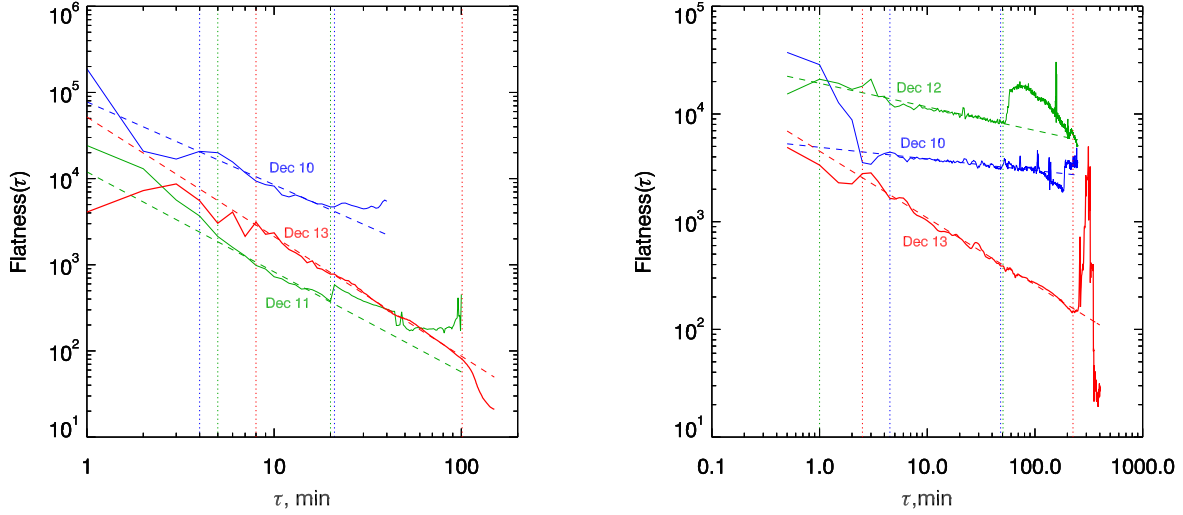


Fig. 6.— *Left*- Flatness functions calculated for three time series of XRT/Be-thin flux marked as Dec 10, Dec 11, and Dec 13. For the set Dec 10, $\kappa = 0.92 \pm 0.05$ inside $\Delta r = (4 - 21)$ min; for the set Dec 11, $\kappa = 1.16 \pm 0.05$ inside $\Delta r = (5 - 20)$ min; for the set Dec 13, $\kappa = 1.39 \pm 0.008$ inside $\Delta r = (8 - 100)$ min. *Right* - Flatness functions calculated for three time series of Nobeyama polarization flux measured at 9.4 GHz. For the set Dec 10, $\kappa = 0.11 \pm 0.004$ inside $\Delta r = (4.3 - 46)$ min; for the set Dec 12, $\kappa = 0.22 \pm 0.006$ inside $\Delta r = (1 - 50)$ min; for the set Dec 13, $\kappa = 0.62 \pm 0.004$ inside $\Delta r = (2.5 - 225)$ min.

4. Photospheric Kinetic Vorticity

Hinode SOT/FG level0 magnetograms are very well suitable for analyzing horizontal displacements of magnetic elements. To measure horizontal displacements of magnetic elements and their speed, we utilized the local correlation tracker (LCT) technique (Strous et al. 1996), which was applied to the same set of SOT/FG magnetograms that we used for intermittency analysis.

The FWHM of the Gaussian tracking window was 9×9 arcsec. This window size was chosen to be an optimum trade off between the noise signal and the spatial resolution of the flow map. A flow map was calculated for each pair of successive images in the data set and is based upon 4 min correlation interval. Our estimation is that the solar noise (an error signal introduced by the evolution of solar features) is less than 30 m s^{-1} . An example of a flow map derived for the magnetogram in Figure 1 (*left*) is shown in Figure 7.

For each flow map we then calculated kinetic vorticity, ω , by using the integral formula:

$$\omega(\mathbf{r}) = \lim_{s \rightarrow 0} \frac{1}{s} \int_L \mathbf{v}_\perp(\mathbf{r}) d\mathbf{l}, \quad (3)$$

where the integration is performed along the contour L enclosing area s that contains a current point \mathbf{r} . In comparison with the traditional differential technique, our approach appears to be more accurate and offers a possibility to integrate using accurate integration methods, such as Simpson formula (http://en.wikipedia.org/wiki/Simpson's_rule).

In our code, the area s was represented by the Gaussian tracking window, $s = \Delta x \times \Delta y$. The components of the transverse velocity, $v_x(i, j)$ and $v_y(i, j)$, were interpolated into a refined mesh of $\Delta x/2 \times \Delta y/2$ pixel size, and then the integration in the CCW direction along the contour $L = [\Delta x, \Delta y, -\Delta x, -\Delta y]$, which encloses a current point $\mathbf{r}(i, j)$, was performed. Integrals along each side of L were calculated by the Simpson's formula. For example, an integral along the positive x -direction (the bottom side of L) was

$$I_1 = \frac{\Delta x}{6} [v_x(m, n) + 4v_x(m + 1, n) + v_x(m + 2, n)]. \quad (4)$$

Here indices m, n belong to the refined mesh, so that $m = 2i$ and $n = 2j$. The sum of four integrals divided by s gives us the estimation of the kinetic vorticity at a current point $\mathbf{r}(i, j)$.

We would like to mention that an analog to the kinetic vorticity is electric current which can be calculated by constituting the flow field v_\perp in Eq. (3) with the horizontal magnetic field B_\perp . Having the map of $\omega(\mathbf{r})$, we calculated the averaged over the area squared kinetic vorticity, $\langle \omega^2 \rangle$. This parameters characterizes the dissipation rate of the kinetic energy in the photosphere caused via random motions of footpoints of magnetic flux tubes.

In Figure 8 we compared the time variation of $\langle \omega^2 \rangle$ and the photospheric intermittency index, κ . The plot shows that there exists a systematic time lag between the two curves with the intermittency being delayed. Cross-correlation analysis showed that the delay is approximately 4 hours. This indicates that the gain of intermittency in the photosphere is preceded by the enhanced rate of kinetic energy dissipation. In other words, the increase in the kinetic vorticity (or self-rotation of plasma structures) leads to subsequent increase of complexity of the photospheric magnetic fields.

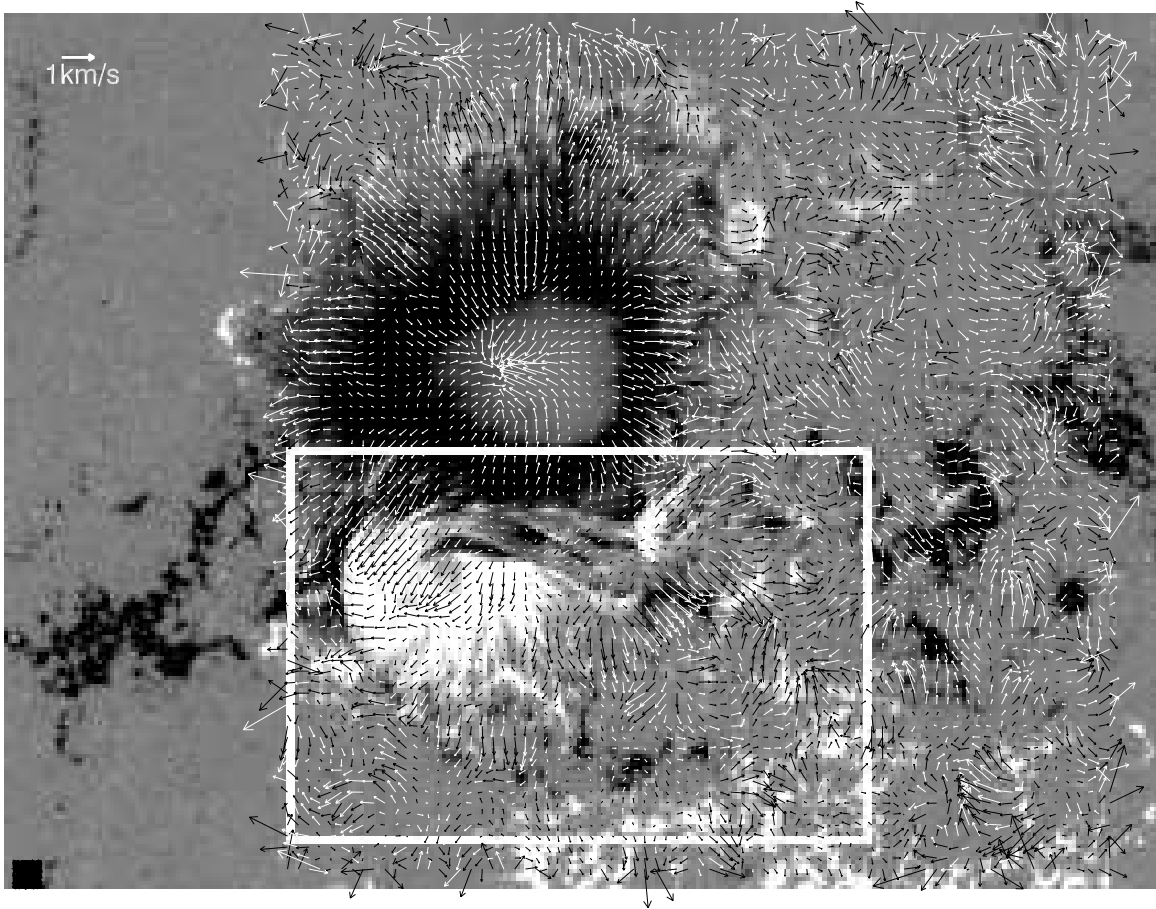


Fig. 7.— Horizontal velocities of magnetic elements derived by the LCT technique for the moment 2006 Dec 12/00:48 UT. Notations are the same as in Figure 1.

5. Discussion and Conclusion

Presented here case study is devoted to the analysis of emergence of a rotating sunspot in the close vicinity of a mature spot of opposite polarity. The fact of the rotation was reported by Nightingale et al. (2007) and is considered as a possible energy source for the X-class flares in this active region. This case demonstrates a rather typical evolution of a delta structure: a highly twisted and stressed magnetic flux rope emerges nearby the pre-existing sunspot. The emerging sunspot of opposite polarity “screws” into the active region magnetic environment. The interaction of the new and old magnetic flux is accompanied by a chain of processes: interchange reconnection at the interaction boundary, propagation of the magnetic stress and helicity into the corona and gain of complexity in chromospheric and coronal magnetic fields. As a result of magnetic reconnections on a variety of spatial scales, new magnetic connections form. Thus, in this particular case of

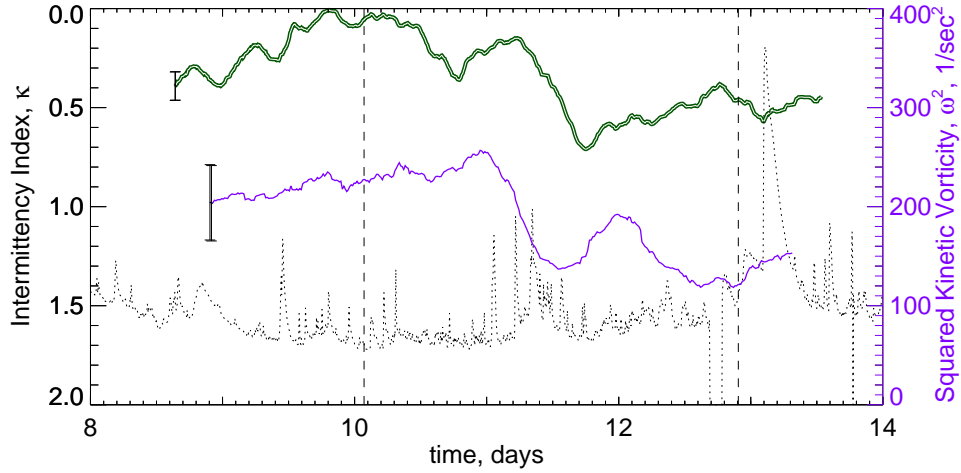


Fig. 8.— *Purple* - Time variations of the squared kinetic vorticity, $\langle \omega^2 \rangle$, averaged over area. *Green* - time variations of the intermittency index, κ , in the photosphere. To ease the comparison, left axis was reversed. *Dotted* line is GOES flux. Other notations are the same as in Figure 2.

NOAA AR 10930, Kubo et al. (2007) reported that one day before the X3.4 flare, Ca H II bright loops began appear near the polarity inversion line. In general, continuous injection of energy and associated magnetic re-arrangements may increase magnetic energy stored in active region. The result often can be a X-class flare, associated with a coronal mass ejection. In NOAA AR 10930 two powerful X-ray flares were observed on Dec 13 and 14, 2006.

What can be added to this scenario from the present research?

The emergence of the rotating sunspot was associated with undulating variations of the squared kinetic vorticity, $\langle \omega^2 \rangle$. The most pronounced peak observed about 2 days before the X3.4 flare was followed by an abrupt fall off. Approximately 4 hours after this enhanced activity of photospheric plasma vorticies we observed a peak of the intermittency index of the photospheric magnetic field. Intermittency can be considered as a measure of complexity of the field and implies the tendency of the field to concentrate into extremely strong, widely separated flux tubes (or sheets) and a burst-like behavior of energy release in time. Intermittency can increase, in particular, due to fragmentation and merging, as well as due to abrupt intrusion of strong entities. We therefore suggest that the abrupt exhausting of strong plasma vorticies presented more freedom for magnetic flux tubes and thus facilitated fragmentation and merging processes, eventually resulting in the gain

of intermittency in the photosphere. Strongly intermittent photospheric magnetic field represents a more stressed magnetic configuration permeated by a multitude of magnetic field discontinuities, which tend to propagate upward due to the magnetic tension.

After the photospheric magnetic intermittency peaked, the chromospheric and coronal intermittency continued to increase during, at least, one more day. Approximately 1.3 days after the peak of photospheric intermittency, the first X-class flare was launched. The data allow us to suggest that the magnetic field first became highly intermittent in the photosphere, and then intermittency had penetrated toward the corona, either due to diffusion of magnetic discontinuities, or due to waves of various types and their interactions. As a result, a highly critical state of the coronal magnetic configuration was reached, the state which at any instant, due to any perturbation, may lead to an eruption.

In the framework of the intermittency concept, the phenomenological scenario for development of a magnetic structure can be regarded as evolution of a non-linear dynamical dissipative system, thus offering a more general insight into the phenomenon. Indeed, a non-linear dynamical dissipative system is believed to evolve toward its attractor, which is a self-organized criticality (SOC) state. The SOC state is characterized by non-rare occurrence of extremely large fluctuations. Which, in turn, results in non-Gaussian distributions of various parameters (recall power-law distributions of flare energy, flare duration, etc., see, e.g., Lu & Hamilton 1991; Charbonneau et al. 2001) and highly intermittent, or, in other words, multifractal organization of the system, as in temporal, so in spatial domain. At the SOC state, any perturbation can provoke an eruption of any size, and thus an eruption cannot be predicted in advance.

Of course, a *short-time* prediction may be quite possible (recall that a snow avalanche, for example, can be "predicted" several seconds in advance by sound), however, this is actually a post factum prediction based on a finite speed of avalanche propagation. The same can be said about hard X-ray precursors of H α flares.

Recently, Leka & Barnes (2007) have come to the conclusion that an individual snapshot of an active region hardly bears information about the time of oncoming flare. In our opinion, this inference perfectly agrees with the concept of non-linear dynamical dissipative system evolution: eruptions cannot be predicted. One can only say that *when* the system reached the SOC state, strong eruptions can happen frequently enough, along with a multitude of smaller ones. One of the ways to make a step ahead is to analyze whether the system reached the SOC state or it is still at the stage of accumulating the energy and complexity? How the SOC state can be reached in the corona and what is the role of the photosphere? In the present study we undertook an attempt tackle these questions. One should keep in mind also that the SOC concept, as any other theory, has

their advantages and disadvantages being under continuous elaboration, see, e.g., Belanger et al. (2007).

As to the usefulness of the intermittency/multifractality concept for understanding of solar phenomena, it is worth to mention the long-standing problem of appearance of low plasma conductivity in the corona, especially during a flare. To explain a solar eruption on the scale of an active region that can last of about 100 minutes, it is necessary to imply the presence of super strong electric currents ($\sim 10^{10} A/km^2$) inside a very thin layers ($< 100 m$, Priest 1982). A fractal concept of coronal magnetic fields can easy meet these requirements. Indeed, a self-similar fractal allows existence of super thin branches (magnetic sheets or tubes) whereas a percolation state, i.e., a large-scale avalanche of the SOC state, implies formation of super strong currents at singular branches of the cluster.

The authors would like to thank the anonymous referee for stimulating discussions and suggestions for improvement of the text. This work was supported, in part, by NASA NNG05GN34G, NASA NNX07AT16G grants, NSF grant ATM-0716512. Hinode is a Japanese mission developed and launched by ISAS/JAXA, with NAOJ as domestic partner and NASA and STFC (UK) as international partners. It is operated by these agencies in co-operation with ESA and NSC (Norway).

REFERENCES

- Abramenko, V. I., Yurchyshyn, V. B., Wang, H., Spirock, T. J., & Goode, P.R. 2002, ApJ, 557, 487.
- Abramenko, V. I., Yurchyshyn, V. B., Wang, H., Spirock, T. J., & Goode, P. R. 2003, ApJ, 597, 1135.
- Abramenko, V. I. 2005a, ApJ, 629, 1141.
- Abramenko, V. I. 2005b, Solar Phys., 228, 29.
- Abramenko, V. I., Pevtsov, A. A., & Romano, P. 2006, ApJ, 646, L81.
- Aschwanden, M. J. 2002, Space Science Rev., 101, 1. =
- Blanger, E, Vincent, A., Charbonneau, P. 2007, eprint arXiv:0708.1941
- Buchlin, E., Vial, J.-C., & Lemaire, P. 2006, Astron. Astrophys., 451, 1091.
- Charbonneau, P., McIntosh, S. W., Liu, H.-L., & Bogdan, T. J. 2001, Solar Phys., 203, 321.

- Conlon, P. A., Gallagher, P. T., McAteer, R. T. J., Ireland, J., Young, C. A., Kestener, P., Hewett, R. J., Maguire, K. 2007, *Solar Physics*, Online First.
- Consolini, G., Berrilli, E., Pietropaolo, E., Bruno, R., Carbone, V., Bavassano, B., & Ceppatelli, G. 1999, in *Magnetic Fields and Solar Processes* (ESA SP-448; Paris: ESA), 209.
- Falconer, D. A., Moore, R. L., & Gary, G. A. 2003, *JGRA*, 108, 1380F.
- Fisher, G.H., Longcope, D.W., Metcalf, T.R., & Pevtsov, A.A. 1998, *ApJ*, 508, 885.
- Frisch, U. 1995, *Turbulence, The Legacy of A.N. Kolmogorov* (Cambridge University Press).
- Georgoulis, M. K., & Rust, D. M. 2007, *ApJ*, 661, L109.
- Golub, L., Deluca, E., Austin, G., and 26 co-authors, 2007, *Solar Phys.*, 243, 63.
- Hagenaar, H. 2001, *ApJ*, 555,448.
- Jing, J., Song, H., Abramenko, V., Tan, C., & Wang, H. 2006, *ApJ*, 644, 1273.
- Klimchuk, J. A. 2006, *Solar Phys.*, 234, 41.
- Kosugi, T., Matsuzaki, K., Sakao, T., and 22 co-authors, 2007, *Solar Phys.* 243, 3.
- Kubo, M., Yokoyama, T., Katsukawa, Y., Lites, B.W., Tsuneta, S., Suematsu, Y., Ichimoto, K., Shimizu, T., Nagata, S., Tarbell, T.D., Shine, R.A., Title, A.M., & Elmore, D. 2007, *PASJ*, 59, S779.
- Kundu, M. R. 1965, *Solar Radio Astronomy* (Interscience Publishers, New York, London, Sydney).
- Leka, K. D., & Barnes, G. 2007, *ApJ*, 656, 1173.
- Lu, E. T., Hamilton, R. J. 1991, *ApJ*, 380, L89.
- Malara, F., & Velli, M. 1994, in *Solar Coronal Structures*, IAU Colloq. 144, eds. V. Rusin, P. Heinzel, and J.C. Vial, VEDA Pub. Comp., 443.
- McAteer, R.T., Gallagher, P.T., & Ireland, J. 2005, *ApJ*, 631, 628.
- Murray, N. 1992, *ApJ*, 401, 386.
- Nightingale, R. W., Schrijver, C. J., Frank, Z. A. 2007, American Astronomical Society Meeting 210, Abstract 94.23

- Priest, E.R. 1982, *Solar Magnetohydrodynamics*, Dordrecht: Reidel.
- Schrijver, C.J., Sandman, A.W., Aschwanden, M.J., & DeRosa, M.L. 2004, *ApJ*, 615, 512.
- Schrijver, C.J., & Title, A.M. 2005, *ApJ*, 619, 1077.
- Spirock, T. J., Yurchyshyn, V. B., & Wang, H. 2002, *ApJ*, 572, 1072
- Stolovitzky, G., & Sreenivasan, K.P. 1992, *Phys. Rev. E*, 48, R33.
- Strous, L. H., Scharmer, G., Tarbell, T. D., Title, A. M., & Zwaan, C. 1996, *Astron Astrophys.*, 306, 947.
- Sudol, J. J., & Harvey, J. W. 2005, *ApJ*, 635, 647.
- Tan, C., Jing, J., Abramenko, V. I., Pevtsov, A. A., Song, H., Park, S.H., & Wang, H. 2007, *ApJ*, 665, 1460.
- Uritsky, V. M., Paczuski, M., Davila, J. M., & Jones, S. I. 2007, *Physical Review Letters*, 99, Issue 2, id. 025001.
- Wang, H., Liu, C., Qiu, J., Deng, N., Goode, P.R., & Denker, C. 2004, *ApJ*, 601, L195
- Wang, H. 2006, *ApJ*, 649, 490.